



## Influence of processing parameters on laser metal deposited copper and titanium alloy composites

Mutiu F. ERINOSHO<sup>1</sup>, Esther T. AKINLABI<sup>1</sup>, Sisa PITYANA<sup>2</sup>

1. Department of Mechanical Engineering Science, University of Johannesburg,  
Auckland Park Kingsway Campus, Johannesburg 2006, South Africa;

2. National Laser Centre, Council for Scientific and Industrial Research (CSIR), Pretoria 0001, South Africa

Received 17 October 2014; accepted 9 May 2015

**Abstract:** The laser metal deposition (LMD) was conducted on copper by varying the processing parameters in order to achieve the best possible settings. Two sets of experiments were conducted. The deposited composites were characterized through the evolving microstructure, microhardness profiling and mechanical properties. It was found that the evolving microstructures of the deposited composites were characterized with primary, secondary and tertiary arms dendrites, acicular microstructure as well as the alpha and beta eutectic structures. From the two sets of experiments performed, it was found that Sample E produced at a laser power of 1200 W and a scanning speed of 1.2 m/min has the highest hardness of HV (190±42) but exhibits some lateral cracks due to its brittle nature, while Sample B produced at laser power of 1200 W and a scanning speed of 0.3 m/min shows no crack and a good microstructure with an increase in dendrites. The strain hardening coefficient of the deposited copper composite obtained in this experiment is 3.35.

**Key words:** copper composites; laser metal deposition; mechanical properties; strain hardening

### 1 Introduction

Laser metal deposition (LMD) is an offshoot of additive manufacturing and an important process in the field of engineering for industrial development. In modern age, LMD has been greatly invested on due to its effectiveness and high efficiency in the repair of complex parts through cladding. The complexity of damaged parts has been taken care of with the application of powder metallurgy in additive manufacturing processes. Precision of repaired component is made easily which reduces or eliminates machining to some extent.

Copper (Cu) is very attractive due to good corrosion resistance, excellent workability, attractive colour, good mechanical properties and the best electrical and thermal conductivity compared with other commercial metals [1]; its corrosion resistance and antimicrobial effect makes it ideal for brewing vessels [2], and an increase in the current density of Cu changes its morphology [3]. Cu is a strong  $\beta$ -stabilizing element and its atomic migration into titanium lattice results in the formation of  $\beta$ -Ti [4].

Several researches have been done in which

different powders have been deposited on titanium alloy (grade 5, Ti6Al4V) substrate with varying laser process parameters to understand the laser-material interactions [5–8]; however, there is a paucity of published literatures on LMD and characterization of Cu composites on titanium alloy (grade 5) substrate. DAO et al [9] presented a computational analysis on the ultrafine crystalline pure Cu with nanoscale growth twins using the pulsed electrodeposition technique at room temperature and laid emphasis on the tensile yield strength from the crystal plasticity model through computational simulations. The deformation characteristics within the grain orientation and the misalignment between the adjacent grains and strain rate sensitivity were studied and characterized. Their results revealed that a decrease in the grain size and the twin spacing leads to an increase in the strength and the ductility of the samples produced [9]. SPASOEVIĆ et al [10] deposited copper on steel from a solution of Cu (II) complex and the coating quality was dependent on the potential difference between the Cu electrode and the steel electrode. A smooth and homogeneous Cu coating was made with good or poor adhesion which

depended on the rate of cementation [10]. FLOEGEL-DELOR [11] also fabricated a Cu stabilizer on a coated conductor, which led to an improvement in the technical and practical performance of the samples during electroplating pulse laser deposition [11]. KHALID et al [12] investigated the microstructural effect of H13 steel powder on high strength Cu substrate via LMD process. They reported that the adhesion between Cu and the steel in the first layer of deposit was more pronounced in the melt pool. The particle size was reduced with an increase in thickness distribution as a result of the process parameters employed and the layer clad. KRISHNA et al [13] predicted the strength of Cu alloy with their derived formula in the study conducted in predicting the strength from the hardness of Cu. The measurement was made in various categories of working heat treatment conditions such as hot working and cold working. They concluded that the accuracy of the strength can be analyzed and estimated using correlations for alloys with low and medium strain-hardening potentials. DASGUPTA et al [14] reported the structural characteristics of titanium coatings produced on Cu substrates. Ti films were deposited on three different substrates which included Cu, glass and silicon substrates at 473 K for 3 h each and these were done in order to optimize the deposition parameters. The thicknesses of the coatings between the interface of the titanium film and the substrate and the intermixing of the elements at the interface were investigated and found to be free from voids.

The motivation for this study is to augmentatively improve and enhance the strain hardening coefficient of Cu, as well as the yield strength and the ultimate tensile strength through LMD process.

In this work, the influence of selected process parameters on the laser metal deposited Cu and Ti6Al4V alloy composites was studied. In the two sets of experiments conducted, the process parameters used included the laser power, scanning speed, powder flow rate and the gas flow rate. The hardness analysis and profiling, yield strength and ultimate tensile strength and the evolving microstructures were investigated.

## 2 Experimental

The experiment was conducted on the ytterbium laser system equipment (YLS-2000-TR) at the National Laser Centre of Council of Scientific Industrial Research (NLC-CSIR), Pretoria, South Africa. The maximum inbuilt power of the laser was 2 kW. The laser equipment was supported with Kuka robot. A three-way nozzle jet was attached to the Kuka robotic arm end. The laser beam radiation passed through the centre of the nozzle

while the powder flowed through the three ways jet. Figure 1 shows a schematic view of the LMD process.

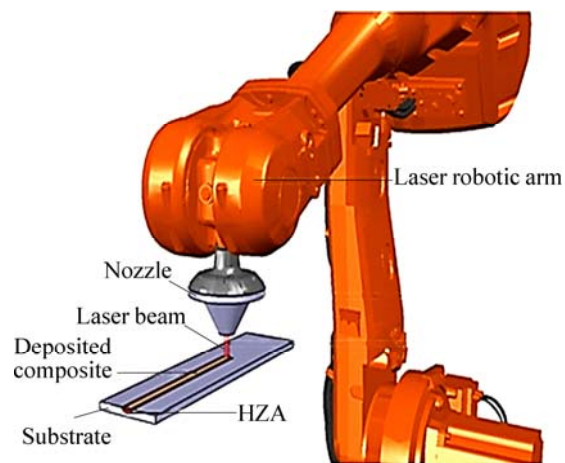


**Fig. 1** Robotic laser showing schematic view of LMD process

From the schematic view shown in Fig. 1, a nozzle was connected to a laser robotic arm. Both the powder and the laser beam were ejected at the end of the nozzle and laser deposit on the substrate to form the solid deposited composite. The heat affected zone (HAZ) and the deposited composite were shown on the substrate as an indication of the deposition process.

### 2.1 Materials and methods

Pure Cu powder and Ti6Al4V substrate were used for the laser experiments. The Cu powder was supplied by Industrial Analytical (Pty) Limited, South Africa. The composition of the Cu powder is shown in Table 1.

**Table 1** Composition and property of Cu powder

Mass fraction/%	Hydrogen loss/%	Apparent density/(g·cm <sup>-3</sup> )
99.83	0.31	5.1

The powder was fed via a hopper, a powder feeder capillary which was connected to the nozzle via a long hose. The particle sizes of the pure Cu powder were between 100 and 200 μm. The powder flowed through the round groove at the base of the hopper assisted by the argon carrier gas. Argon gas was supplied at 10 L/min to provide a shield for the deposited composite during the operation so as to prevent oxygen contamination.

A square plate with dimensions of 102 mm × 102 mm × 7.54 mm containing 99.6% Ti6Al4V alloy was used for the substrate. The substrate was sand blasted prior to deposition process in a cubicle to create rough surface for metallographic bonding between the composite and the substrate. Surface cleaning was achieved with acetone and dried off. As shown in Table 1, almost 100% of the Cu powder was present in the

compositional variation.

The experimental matrix used in the first set of experiments is presented in Table 2. The laser power, the powder flow rate and the gas flow rate were kept constant while the scanning speed was varied. The process parameters used in the second set of experiments are also presented in Table 2. The scanning speed, the powder flow rate and the gas flow rate were kept constant while the laser power varied.

**Table 2** Process parameters for first and second sets of experiments

Sample designation	Laser power/W	Scanning speed/(m·min <sup>-1</sup> )	Powder feed rate/(r·min <sup>-1</sup> )	Gas flow rate/(L·min <sup>-1</sup> )
First	A	1200	0.1	2.0
	B	1200	0.3	2.0
	C	1200	0.5	2.0
	D	1200	0.9	2.0
	E	1200	1.2	2.0
Second	F	600	0.3	1.5
	G	900	0.3	1.5
	H	1200	0.3	1.5
	I	1500	0.3	1.5
	J	1800	0.3	1.5

For the two sets of experiments, the beam diameter of 4 mm and a focal length of 210 mm were used throughout the experiments. The standoff distance between the nozzle and the substrate was kept at 12 mm. Altogether, ten deposits were made on the substrates and labelled as Samples A–J. The deposited composites were wire-brushed to clear the surface powders on them. The substrate containing the deposit was marked out and cut to size for mounting purpose. The samples were mounted in polyfast hot mounting resin. All the samples were ground and prepared for metallography according to the E3–11 ASTM standard [15].

## 2.2 Microstructure

The etchant used was prepared for both the substrate and the Cu composite. Kroll's reagent was prepared for the Ti6Al4V alloy substrate with 100 mL distilled H<sub>2</sub>O, 2 mL HF and 4 mL HNO<sub>3</sub> and the reagent for the deposited Cu composite was prepared with 5 mL distilled H<sub>2</sub>O, 5 mL NH<sub>3</sub> solution and 3 mL H<sub>2</sub>O<sub>2</sub> [16]. Each sample was etched for 15 s for the Ti6Al4V substrate, rinsed under running water and dried off. The second etching was done on the Cu deposited composite for 5 s, and rinsed again under running water prior to optical observation. All the samples were observed on a BX51M Olympus microscope at low and high magnifications.

## 2.3 Microhardness profiling

A Vickers microhardness machine Zwick/Roell at the University of Johannesburg, Doornfontein Campus, South Africa, was used for the hardness tests. The indentations were made from the top of the deposit to the interface and to the substrate. Nine indentations were made on each sample laterally. A load of 200 g and a dwell time of 15 s were used according to AKINLABI [17]. The distance left between indentations was 150 μm. The hardness was conducted according to E384–11e1 ASTM standard [18].

## 2.4 Yield strength and ultimate tensile strength

The yield strength (YS,  $\sigma_{0.2}$ ) was calculated from the relationship evaluated by KRISHNA et al [13] in the prediction of the strength from hardness for copper alloys. The yield strength (YS) and the ultimate tensile strength (UTS,  $\sigma_b$ ) were calculated using the following equations:

$$\sigma_{0.2}=2.874H \quad (1)$$

$$\sigma_b=3.353H \quad (2)$$

The correlation between the  $\sigma_{0.2}$  and the hardness  $H$  was determined by Eq. (1) and the correlation between the  $\sigma_b$  and the  $H$  was determined by Eq. (2). The strain hardening coefficient of the pure copper used for this experiment was evaluated by dividing  $\sigma_b$  by  $\sigma_{0.2}$  [13].

## 3 Results and discussion

### 3.1 Physical appearance of deposited samples

The physical studies of the deposited samples A–J for the two sets of experiments are shown in Fig. 2. Meanwhile, Figs. 2(a) and (b) are of the same composites. Figure 2(a) shows the clad produced in the second set of experiment. From the physical appearance of the deposited samples, Fig. 2(a) indicated that the deposit track of Sample J had a zero bonding between the deposited composite and the substrate. Here, a laser power of 1800 W and a scanning speed of 0.3 m/min were used. The poor bonding can be attributed to the high laser power employed which was too high to create good bonding between the coating and the substrate. Although the melt pool was created in the substrate, the composite was delaminated at the end of deposit. The powder flow rate and the gas flow rate used were in the appropriate proportion and they were not liable for the poor bonding. The delamination of Sample J would occur as a result of a very high heat input into the sample during deposition. Some bubbles were observed on the surface of Sample J as a result of the heat input applied and the cooling rate. The cooling at the top of the deposited composite solidified the bubbles, thereby creating a bubble-like surface.

Figure 2(b) shows the same composite with the delamination of the first deposit in the same second set of experiment. This showed the pull-out of the deposited composite from the substrate and leaving the shape of the pull-off in the substrate. The pulled-out was as a result of lack of good adhesive bonding produced by the laser power of 1500 W used for the deposition process. The deposited composite (Sample I) was also delaminated during the cutting process for metallographic preparation as it indicated a minimal bonding prior to cutting. Figure 2(c) depicts the deposited samples for the first set of experiment with a constant laser power of 1200 W and the samples are labelled as A to E.

### 3.2 Powders morphology

Figure 3(a) shows the morphology of Cu powder observed under the SEM. The morphology indicates a spherical particle shaped bimodal structure. The morphology is spherically equiaxed and bimodal in structure. Figure 3(b) shows the SEM image of Ti6Al4V substrate. It shows the microstructure of the rolled Ti6Al4V substrate. The microstructure consists of the alpha ( $\alpha$ ) and beta ( $\beta$ ) phase structures. The darker phases are the  $\alpha$ -phase while the lighter phases are the  $\beta$ -phase.

Figure 4 shows the particle size distribution of the Cu powder which was conducted on the Microtrac

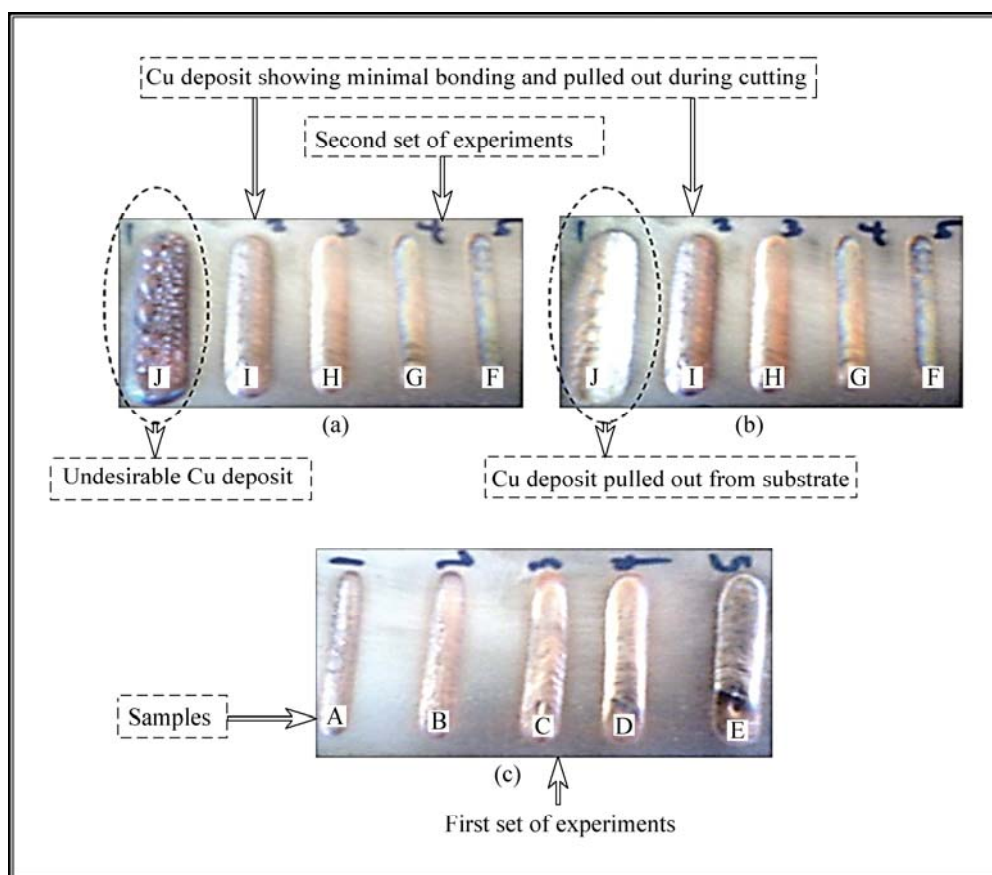


Fig. 2 Physical appearance of deposited Samples A–J

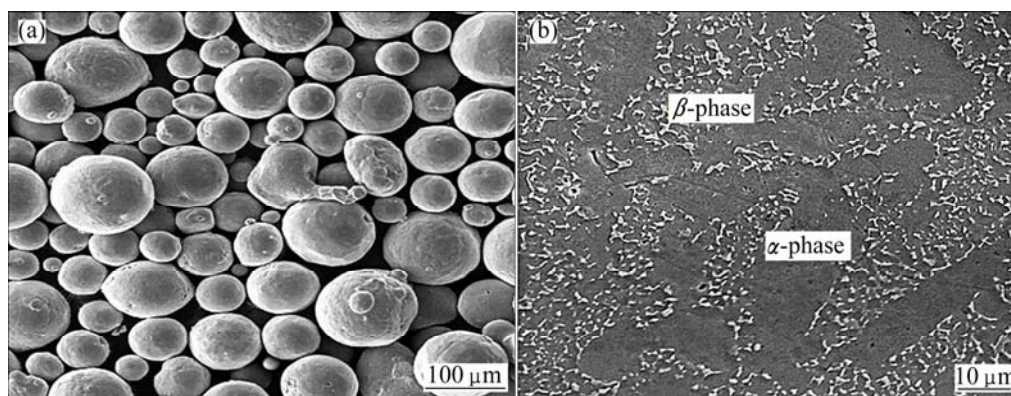
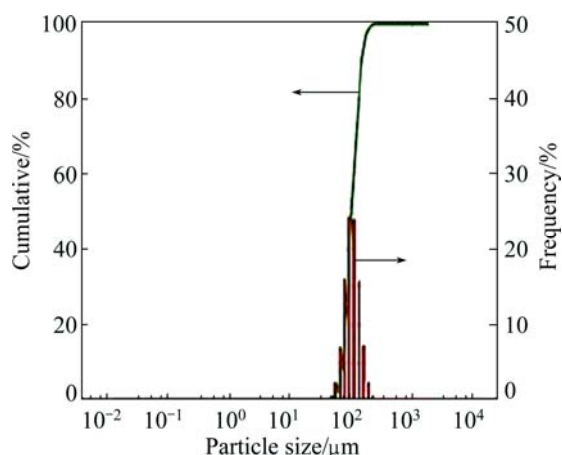


Fig. 3 SEM morphologies of Cu powder (a) and Ti6Al4V substrate (b)



**Fig. 4** Particle size distribution of Cu powder

analyser. The distribution showed the particle size between 100 and 300  $\mu\text{m}$  respectively.

### 3.3 Microstructural analysis

The microstructures of Samples A–G were observed at low and high magnifications under the optical microscope. Figure 5(a) shows the microstructure of Sample A at a laser power of 1200 W and a scanning speed of 0.1 m/min. Dendrites were formed randomly throughout the deposited Cu composite. Between the interface of the deposited Cu and the substrate, acicular structures were also observed, which resulted in parallel little cracks at the interface. Figure 5(b) shows the microstructure of Sample A focused at a high magnification. The dendrite arms formed consisted of the primary, secondary and tertiary arms. The primary arm was found to be richer in Cu, which showed a compositional gradient from the inner region of a dendrite arm to the outer surface [19]. The black structures found in the dendrite arms were the infill of  $\alpha+\beta$  eutectic structure.

Figure 5(c) shows the microstructure of Sample B. The dendrites show an increase in thickness as the scanning speed increases and the interface between the Cu deposit and Ti6Al4V substrate shows good bonding. Sample B focused at a high magnification as shown in Figure 5(d) shows that the primary dendrite arms grow thicker and the tertiary arms grow shorter. Figure 5(e) shows the microstructure of Sample C formed at a laser power of 1200 W and a scanning speed of 0.5 m/min. Snowflakes of dendrites formed immediately after the acicular microstructures and at this point, the dendrites disappeared and the acicular microstructures formed at the interface of Cu composite and substrate became stronger and showed pin-like and sharp edges. The cracks prevailed due to the fact that Ti6Al4V substrate created a disagreement between the bonding as a result of the low heat input involved. The formation of these

sharp acicular microstructures from the substrate into the Cu composite tended to create a form of dissociation. This sharpness happened at high laser power. Very high laser pulled away the Cu composite because of the energy dissipated within the acicular microstructure.

As the scanning speed was kept on increasing, the dendrites of the primary and secondary arms disappeared, as shown in Fig. 5(f) of the Sample C observed at a higher magnification. Figure 5(g) shows the total disappearance of the dendrite structure in Sample D with further increase in scanning speed. Dendrites were always visible for slowly cooled structures and at a fast rate of cooling, the dendrites were found to be invisible [19]. The infill of  $\alpha+\beta$  eutectic structure was also found to disappear as the dendrite arm disappeared after new solidification sites were formed. Figure 5(h) shows the microstructure of Sample E. The acicular structure found at the interface grew taller, thereby creating more cracks to prevail. A thin layer of Cu composites was cladded on the substrate at high scanning speed of 1.2 m/min and the thin layer formed led to a fast cooling rate of Sample E. The sharp acicular microstructures were responsible for the lateral cracks. Their sharpness actually quaked the composite, thereby creating the lateral cracks and also enhanced embrittlement. Figure 5(i) shows Sample F produced at a laser power of 600 W and a scanning speed of 0.3 m/min. The dendrite arms formed consisted of the primary, secondary, and tertiary arms. The primary arms grew thicker while the secondary and the tertiary arms grew shorter. Figure 5(j) shows Sample G at a laser power of 900 W and a scanning speed of 0.3 m/min. There was a growth of acicular structure from the top of the deposit and also from the Cu deposit and substrate interface. Cracks were also observed in the deposited composites. The microstructures of Sample H were not captured due to the flat and low volume of the deposited composite formed and the coated surface consisted of lateral cracks.

### 3.4 Microhardness profiling

The Vickers microhardness profiles were obtained and the average values are presented in Table 3. Table 3 shows the average hardness and the standard deviations of Samples A–H, respectively. The hardness values of Samples I and J were not obtained due to poor and zero bonding between the coat and the substrate interface. So, the hardness was neglected. Lateral cracks and breakages were observed on Sample H under microscope. The hardness test started at the interface of the composite and the substrate. The average hardness of Sample H did not account for the deposited Cu hardness values, but it indicated the indentation value of the heat affected zone, fusion zone and the Ti6Al4V substrate. The microhardness (HV) values indicated an increase as the

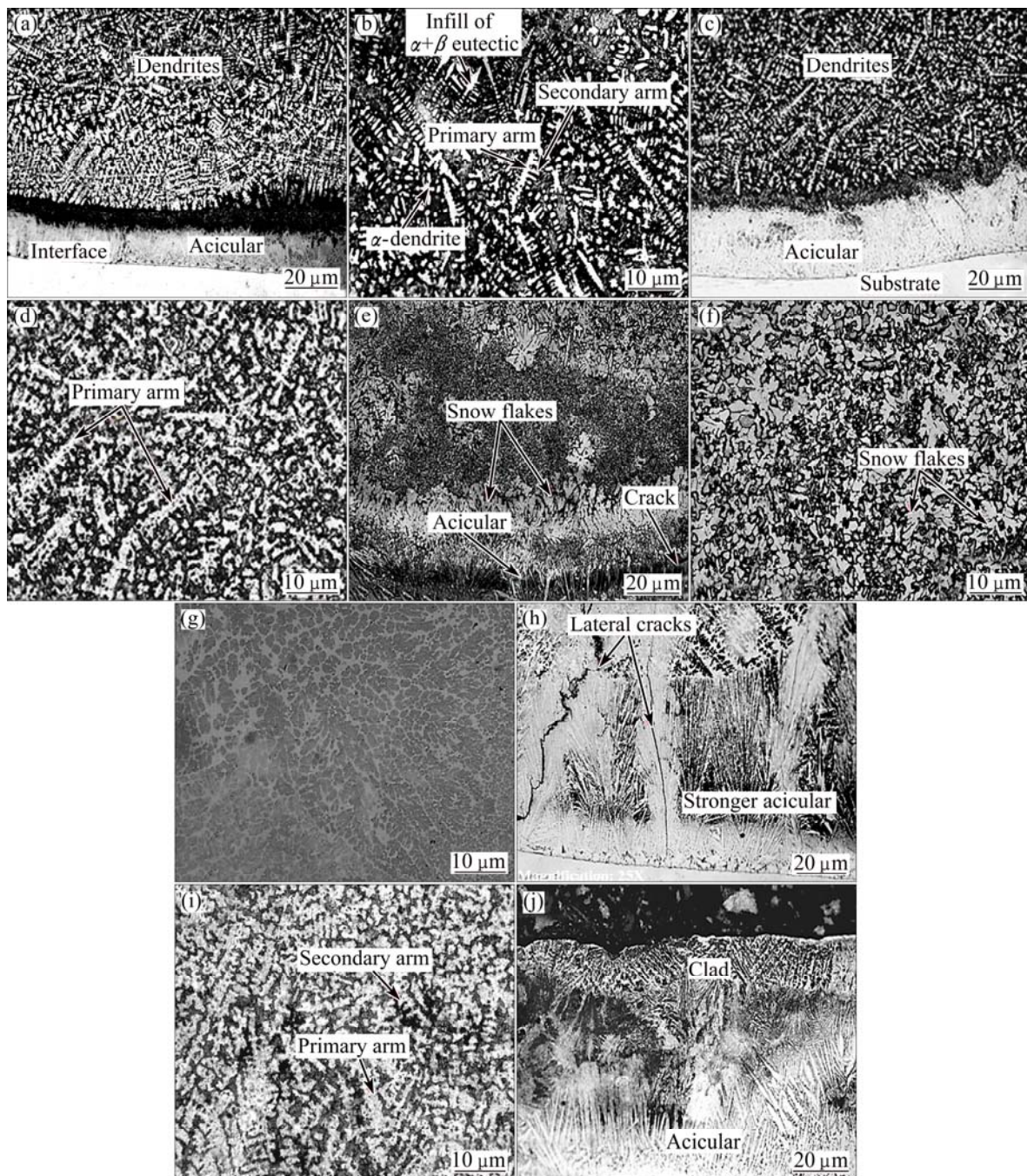


**Fig. 5** Microstructures of Samples A (a, b), B (c, d), C (e, f), D (g), E (h), F (i) and G (j) showing primary, secondary and tertiary arms dendrites, acicular microstructure as well as  $(\alpha+\beta)$  eutectic structures surrounding dendrites of  $\alpha$ -phase

**Table 3** Average hardness of Samples A–H

Sample No.	A	B	C	D	E	F	G	H
Average hardness (HV <sub>0.2</sub> )	144±16	146±13	161±19	164±17	190±42	140±18	155±20	139±13

scanning speed increased from Samples A to E between 0.1 m/min and 1.2 m/min. Samples F to J were laser-deposited with varying laser power between 600 W and 1800 W and a constant scanning speed of 0.3 m/min. Table 3 shows an increase in the average hardness value of the deposited Samples A–E as the scanning speed

increases. During the laser deposition process, Sample J was delaminated from the substrate and Sample I was dissociated during the cutting process. The average hardness values between Samples A and B were increased by about 1.4%. Between Samples B and C, the average hardness was increased by about 10% while

Samples C and D showed an average hardness increase of approximately 2% and the average hardness value variance between Samples D and E was about 16%. All these increments in the hardness values were the result of the increment in the scanning speed. As the scanning speed increased, the flow of Cu powder delivery in the melt pool of the substrate was reduced, thus the time required to melt the powder was too short and the cooling rate was very fast. This in turn created smaller and shorter grain boundaries since there was no room for grain migration to form new grains during the laser–material interactions. A similar trend of increase in hardness was also observed between Samples F and G, that is, an increase in the laser power also led to an increase in the hardness value. Table 3 also illustrates an increase in the hardness value between Samples F and H. At a point, a decrease in hardness occurred as the laser power was kept on increasing. This is in agreement with a preliminary study Ref. [20].

As the laser power increased, the melting of the powders also increased and this consequently led to the migration of the grain boundaries with another in order to form new grains. This phenomenon improved the ductility of a material.

Figure 6 shows the plot of hardness profiling of Samples A–H. The profiling shows the following three phases: the hardness of the Cu deposited composite, the interface hardness between the Cu deposit and the substrate and the indentations made on the substrate. The hardness showed a decrease on each sample and increased towards the interface. The hardness profiles increased drastically which showed some peaks at the interface, indicating a very high hardness at the interface. This upshot in the middle was as a result of the energy generated by the acicular structure between the substrate and the clad at high laser power.

The higher hardness at the interface could be as a result of the force-action and strength interchange between the interface of the Ti6Al4V substrate and the

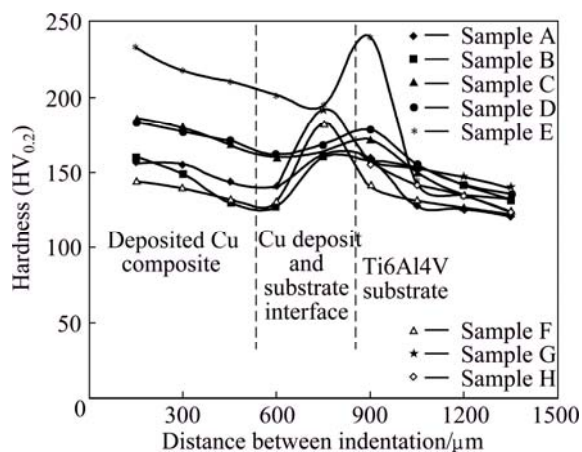


Fig. 6 Hardness profilings of deposited Cu composites

Cu composites. The hardness profiles further decreased immediately in the interface region since the lateral inner part of substrate was not affected by heat, but the hardness values increased as the scanning speed increased for each sample.

### 3.5 Yield strength and ultimate tensile strength

The YS and UTS were calculated using the formula adopted by KRISHNA et al [13] in Eqs. (1) and (2). This principle occurs from the relationship of a linear straight line analysis. Figure 7 shows the plot of the YS and UTS against the hardness of all the samples, which indicates an increase in both the YS and UTS as hardness increases. The ratio of the UTS to YS is 3.35, which was employed to verify the effect of strain hardening on the Cu-deposited composites. Each hardness value of every indentation was substituted into Eqs. (1) and (2) to obtain the YS and the UTS. Dividing each UTS by YS, the strain hardening coefficient amounts to be 3.35. The graph is a perfectly straight line that passes through the origin if it is traced to the zero point. According to PAVLINA and TYNE [21], the strain hardening of a material for UTS/YS ratio greater than 1.52 is considered to be high. The Cu deposited composites in this study showed a high UTS/YS ratio of 3.35.

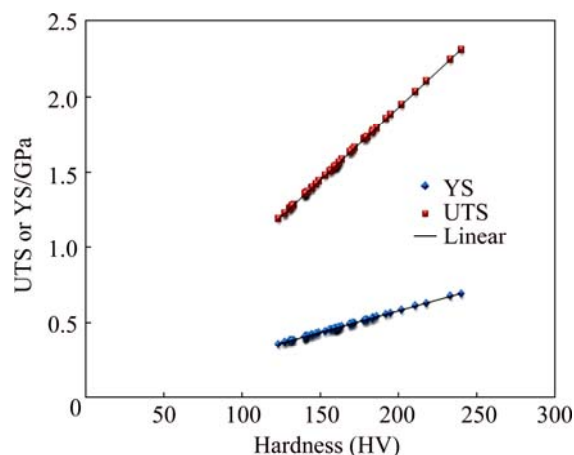


Fig. 7 Plot of YS and UTS against hardness value

The correlation between the YS and UTS from the plot apparently shows the trend lines to be close. This is in agreement with the study of KRISHNA et al [13], and all the points were observed to be on the lines, which also indicated a zero point of intersection. The YS for pure Cu ranged between 300 and 700 MPa, which was also in line with the prediction made by KRISHNA et al [13] on the strength of Cu alloys covering a range of 50 to 1200 MPa. The UTS for predicting the strength of the Cu alloy falls between 200 and 1400 MPa. The hardness and strength values of the Cu alloys in Ref. [13] were processed by solid solution strengthening, precipitation hardening, cold working, and dispersion

strengthening. This present study illustrated the characterization of laser deposited Cu composites and showed a greater improvement in strength more than the processes used in Ref. [13]. In this study, the UTS of pure Cu composites ranged between 1100 and 2400 MPa and all the 43 measurements of hardness altogether were put into consideration for the analysis.

#### 4 Conclusions

1) The deposition of Cu powder on Ti6Al4V substrate was investigated and characterized. The laser deposited Cu composites showed an enhancement in the mechanical properties.

2) The physical appearances of the composites revealed that the deposited Cu composites with laser powers of 1500 and 1800 W at a scanning speed of 0.3 m/min have zero bonding between the Cu deposit and the substrate. So, these parameters should be avoided in future experiments.

3) The Vickers microhardness values of the samples in the first set of experiments range between HV (144±16) and HV (190±42), while in the second set of experiment, they range between HV (139±13) and HV (155±20). The YS and UTS values of Sample E were observed to be higher, with 690 MPa and 2313 MPa, respectively.

4) The microstructural analyses revealed a decrease in the formation of dendrites as the scanning speed increased and disappeared at some points due to the fast cooling rate.

5) The strain hardening coefficient of the deposited Cu composite obtained in this experiment was 3.35 and can be considered an improvement compared with other means of fabrication or production.

#### Acknowledgments

This work is supported by the Council of Scientific and Industrial Research (CSIR), National Laser Centre, Rental Pool Programme, Pretoria, South Africa and also for the award of the Africa Laser Centre bursary to the main author.

#### References

- [1] LENNTECH B V. Water treatment solution. Lenntech [EB/OL]. 2013–10–12. [www.lenntech.com/periodic/element/Ti](http://www.lenntech.com/periodic/element/Ti).
- [2] JOLLY J L. The US copper-base scrap industry and its by products: An overview. Copper development association [EB/OL]. 2013–09–03. [http://www.copper.org/publications/pub.list/pdf/scrap\\_report.pdf](http://www.copper.org/publications/pub.list/pdf/scrap_report.pdf).
- [3] MAKSIMOVIĆ V, PAVLOVIĆ L, PAVLOVIĆ M, TOMIĆ M. Characterization of copper powder particles obtained by electro-deposition [J]. Metalurgija, 2009, 15(1): 19–27.
- [4] GHOSH M, CHAUERJEE S. Diffusion bonded transition joints of titanium to stainless steel with improved properties [J]. Material

- Science Engineering A, 2003, 358: 152–158.
- [5] AKINLABI E T, MAHAMOOD R M, SHUKLA M, PITYANA S. Effect of scanning speed on material efficiency of laser metal deposited Ti6Al4V [C]//Proceedings of World Academy of Science, Engineering and Technology. Waset, Turkey, 2012: 1531–1535.
- [6] SUN Y, MINGZHONG H. Statistical analysis and optimization of process parameters in Ti6Al4V laser cladding using Nd:YAG laser [J]. Optics and Lasers in Engineering, 2012, 50: 985–995.
- [7] MAHAMOOD R M, AKINLABI E T, SHUKLA M, PITYANA S. Laser metal deposition of Ti6Al4V: A study on the effect of laser power on microstructure and microhardness [C]//Proceedings of International MultiConference of Engineers and Computer Scientists. Hong Kong: Newswood Limited, 2013: 994–999.
- [8] YU J, ROMBOUITS M, MAES G, MOTMANS F. Material properties of Ti6Al4V parts produced by laser metal deposition [J]. Physics Procedia, 2012, 39: 416–424.
- [9] DAO M, LU L, SHEN Y F, SURESH S. Strength, strain-rate sensitivity and ductility of copper, with nanoscale twins [J]. Acta Materialia, 2006, 54: 5421–5432.
- [10] SPASOJEVIĆ M, CVIJOVIĆ M, RYBIĆ-ZELENOVIĆ L, AĆAMOVIĆ-JOKOVIC G. Electrochemical deposition of copper on steel from a solution of diacido-1,3 propylenediamine-*N*, *N*-diacetato-*N*, *N*-dipropionate cuprate (II) [J]. Applied Chemistry, 2007, 80(4): 566–570.
- [11] FLOEGEL-DELOR U, RIEDEL T, WIPPICH D, GOEBEL B, ROTHFELD R, SCHIRRMMEISTER P, WERFEL F N, USOSKIN A, RUTT A. Reel-to-reel copper electroplating on pulse laser deposition coated conductor [J]. IEEE Transactions on Applied Superconductivity, 2011, 21: 2984–2987.
- [12] KHALID M I, MASOOD S H, BRANDT M. Microstructural investigation of direct metal deposition of H13 steel on high strength copper substrate [C]//Proceedings of World Congress on Engineering. Hong Kong: Newswood Limited, 2009: 704–708.
- [13] KRISHNA S C, NARENDRA K G, JHA A K, BHANU P. On the prediction of strength from hardness for copper alloys [J]. Materials, 2013, 2013: 352578.
- [14] DASGUPTA A, SINGH A KUMAR PARIDA P, RAMASESHAN R, KUPPUSAMI P, SAROJA S, VIJAYALAKSHMI M. Structural characteristics of titanium coating on copper substrates [J]. Bull Material Science, 2011, 34(3): 483–489.
- [15] ASTM E3-11. Guide for preparation of metallographic specimens [S].
- [16] TAYLOR B. Metallographic preparation of titanium: Struers application note on titanium [EB/OL]. 2013–08–11. [http://www.struers.com/resources/elements/12/104827/Application\\_Note\\_Titanium\\_English.pdf](http://www.struers.com/resources/elements/12/104827/Application_Note_Titanium_English.pdf).
- [17] AKINLABI E T. Characterisation of dissimilar friction stir welds between 5754 Al alloy and C11000 copper [D]. Port Elizabeth: Nelson Mandela Metropolitan University, South Africa, 2010.
- [18] ASTM E384–11e1. Standard test method for knoop and vickers hardness of materials [S].
- [19] SCOTT D A. Metallography and microstructure of ancient and historic metals [M]. Singapore: Tien Wah Press Limited, 1991: 155.
- [20] ERINOSHO M F, AKINLABI E T, PITYANA S. Laser metal deposition of Ti6Al4V/Cu composite: A study of the effect of laser power on the evolving properties [C]//Proceedings of the World Congress on Engineering. Hong Kong: Newswood Limited, 2014: 1202–1207.
- [21] PAVLINA E J, van TYNE C J. Correlation of yield strength and tensile strength with hardness for steels [J]. Materials Engineering and Performance, 2008, 17(6): 888–893.

## 工艺参数对激光金属沉积铜钛合金复合材料的影响

Mutiu F. ERINOSHO<sup>1</sup>, Esther T. AKINLABI<sup>1</sup>, Sisa PITYANA<sup>2</sup>

1. Department of Mechanical Engineering Science, University of Johannesburg,  
Auckland Park Kingsway Campus, Johannesburg 2006, South Africa;

2. National Laser Centre, Council for Scientific and Industrial Research (CSIR), Pretoria 0001, South Africa

**摘要:** 为获得最佳设计方案, 设计两种实验方案, 通过改变工艺参数对铜钛合金复合材料进行激光金属沉积。从显微组织演变、硬度和力学性能三方面对所沉积的复合材料进行表征。结果表明: 复合材料的显微组织由一次、二次和三次枝晶臂, 针状组织和  $\alpha+\beta$  共晶组织组成。两种实验方案结果表明, 在激光功率为 1200 W、扫描速率为 1.2 m/min 的条件下得到的样品 E 具有最高的硬度, 其值为 HV (190±42), 但由于其脆性, 因此出现一些横间裂纹; 而在激光功率为 1200 W、扫描速率为 0.3 m/min 条件下得到的样品 B 无裂纹产生, 且其显微组织良好并含有较多的枝晶。得到的铜复合材料的应变硬化系数为 3.35。

**关键词:** 铜复合材料; 激光金属沉积; 力学性能; 应变硬化

(Edited by Wei-ping CHEN)